Research Article J. Electrochem. Sci. Technol., 2022, 13(4), 417-423

Highly Active Electrocatalyst based on Ultra-low Loading of Ruthenium Supported on Titanium Carbide for Alkaline Hydrogen Evolution Reaction

Junghwan Kim†, Sang-Mun Jung†, Kyu-Su Kim, Sang-Hoon You, Byung-Jo Lee, and Yong-Tae Kim*
Department of Materials Science and Engineering, Pohang University of Science and Technology (POSTECH), Pohang 37673, Republic of Korea

ABSTRACT

With the emerging importance of catalysts for water electrolysis, developing efficient and inexpensive electrocatalysts for water electrolysis plays a vital role in renewable hydrogen energy technology. In this study, a 1nm thickness of TiC-supported Ru catalyst for hydrogen evolution reaction (HER) has been successfully fabricated using an electron (E)-beam evaporator and thermal decomposition of gaseous CH_4 in a furnace. The prepared Ru/TiC catalyst exhibited an outstanding performance for alkaline hydrogen evolution reaction with an overpotential of 55 mV at 10 mA cm^{-2}. Furthermore, we demonstrated that the outstanding HER performance of Ru/TiC was attributed to the high surface area of the support and the metal-support interaction.

Keywords : Alkaline Water Electrolysis, Hydrogen Evolution Reaction, Ruthenium, Titanium Carbide, Metal-Support Interaction

Received : 4 March 2022, Accepted : 25 March 2022

1. Introduction

The rapid development of renewable energy use is accelerating the global energy transformation [1,2]. To increase this momentum and reduce emissions, hydrogen has been developed as an alternative energy carrier. In particular, the Earth's abundant water can guarantee hydrogen production in a sustainable way, and therefore, water-electrolysis technology would be considered a primary ecofriendly hydrogen-production method. A water-electrolysis reaction involves two half-cell reactions; an oxygen evolution reaction (OER) and a hydrogen evolution reaction (HER) at the anode and the cathode of the general water-electrolysis cell, respectively. Both reactions are vital in water-electrolysis, and thus, developing efficient and inexpensive electrocatalysts for OER and HER plays an important role in renewable hydrogen energy technology [3].

In terms of HER, Pt-based precious materials have been considered the most effective electrocatalyst. Nevertheless, the high cost and scarcity of Pt (Pt = \$34 g^{-1}, Mar 2022) is a challenging obstacle to the large-scale commercialization of water electrolysis [4-7]. So far, numerous materials design strategies have been proposed for HER to secure low-cost and high-activity electrocatalysts. The first category is improving the performance of noble metal-free electrocatalysts [8-11]. Though using the non-precious metal electrode such as Ni drastically lowers the manufacturing cost of catalysts [12], it is hard for these transition metals to achieve high performance as platinum due to their sluggish kinetics [13,14]. The second category is minimizing the amount of noble-metal loading in the electrocatalyst while retaining the catalytic activity. A cost-effective electrocatalyst has recently been developed by fabricating a catalyst in which noble metal is extremely dispersed in atomic units such as Ru [15-17], Ir [15,18], and Pd [19-21]. Among these rare elements, Ru is a notable candidate for replacing platinum due to its good HER

†These authors contributed equally to this work
*E-mail address: yongtae@postech.ac.kr

DOI: https://doi.org/10.33961/jecst.2022.00178

activity and relatively low cost compared to Pt or other possible candidates (Ru = \$17 g^{-1}, Mar 2022) [22-24].

In particular, the excellent water dissociation capability of Ru can increase the possibility of replacing Pt with Ru as a HER electrocatalyst under alkaline conditions. Pt shows a relatively good HER performance in acid electrolytes; however, it experiences sluggish kinetics in alkaline media. This catalytic activity restriction of Pt generally arises from the fact that they are inefficient in the stages of water dissociation [25-29]. In contrast, Ru has a high water dissociation capability due to its oxophilicity, which can be extended to using Ru-based materials in alkaline HER [30].

In this study, we introduce an efficient alkaline HER electrocatalyst with an ultra-low loading of Ru on titanium carbide (TiC). We successfully fabricated a 1 nm thickness of TiC-supported Ru catalyst for HER by using an electron (E)-beam evaporator, which is a nanoscale physical vapor deposition (PVD) device. TiC was easily formed using the thermal decomposition method, and it shows highly porous surface structures compared to Ti metal or other Ti compounds (oxide, carbide, and nitride). Furthermore, this TiC-supported Ru catalyst exhibited a high HER activity with an overpotential of 55 mV at a current density of 10 mA cm^{-2}, demonstrating the outstanding HER performance of Ru/TiC.

2. Experimental

2.1 Model catalyst preparation

Polycrystalline metal pellets were prepared, mechanically polished using sandpaper (silicon carbide, MICROCUT®, Buehler) and alumina powder (0.05 μm, BASi), and then cleaned by sonication in deionized water for 30 min. Next, the polished Ti pellets (99.99%, diameter = 6.35 mm, Kurt J. Lesker Co. Ltd.) were annealed in a radio frequency (RF) furnace (Ambrell, Easyheat 0224). The annealing process was conducted under Ar (5%)–H_2, air, Ar (10%)–CH_4, and Ar (10%)–NH_3 for metallic Ti, TiO_2, TiC, and TiN, respectively. Before annealing, each gaseous reactant was saturated in the furnace for 10 min. Each sample was then annealed for 300 s. Metallic Ti, and TiC formed at 500–700°C, while TiO_2 and TiN were obtained at 600–800°C and 500–700°C, respectively. The annealed substrate samples were then naturally cooled down at room temperature for 10 minutes at the same gas flow. After the substrate fabrication and characterization, Ru deposition was conducted using E-beam deposition (Korea Vacuum Tech), a PVD method that features more precise controllability than other PVD types such as magnetron sputtering. Ru (1 nm) was deposited on each substrate sample, and a Ru metal target was used for the deposition process. Ru 1 nm deposited on glassy carbon (GC), Polycrystalline Pt pellet (99.999%, diameter = 6.35 mm, Kurt J. Lesker Co. Ltd.) and Ru pellet (99.999%, diameter = 6.35 mm, Kurt J. Lesker Co. Ltd) were also prepared as a reference for comparison of HER activity.

2.2 Powder catalyst preparation

Powder Ru/TiC samples were also prepared by powder sputtering to experimentally investigate the atomic fraction of Ru. Titanium carbide nanopowder (Sigma-Aldrich, particle size < 200 nm) was prepared to fabricate the substrate. TiC powder (10 mg) was ground in the mortar and placed in the sputtering chamber, and Ru deposition was then conducted for 3, 9, and 12 min under an Ar flow of 0.5 sccm. Next, each powder sample was added to a mixture consisting of deionized water, isopropyl alcohol (DAEJUNG), and Nafion® perfluorinated resin solution (Sigma-Aldrich) at a ratio of 79.6:20:0.4 so that every catalyst solution contained 20 $\mu g_{Ru\ (or\ Pt)}$ cm^{-2}. Finally, these solutions (20 μL) were loaded on the glassy carbon disk electrode pellets (GC, 99.99%, diameter = 5 mm, Kurt. J. Lesker Co. Ltd) to be gone through the electrochemical tests. For comparison, Pt/C (20wt%) and Ru/C (5wt%) were also prepared as a reference for the electrochemical tests.

2.3 Electrochemical measurements

The electrochemical properties of the Ti-compound substrate samples were measured using a Potentiostat (Metrohm Autolab, AUT51660) with a standard three-electrode electrochemical cell using a rotating disk electrode setup (RDE, PINE research) at room temperature. Mercury/mercury oxide (Hg/HgO, RE-61AP, ALS) and graphite rod were used as a reference and counter electrodes, respectively. KOH (1 M, DAEJUNG) was used as an alkaline electrolyte (pH = 14). To remove the side effects of oxygen perfectly, we purged the Ar gas to the electrolyte for

more than 30 min before running all electrochemical tests. Cyclic voltammetry (CV) tests were conducted for the substrates at a scan rate of 0.05 V s^{-1} and a potential range of 0.05–1.2 V *vs.* reversible hydrogen electrode (RHE). Linear sweep voltammetry (LSV) tests were conducted at a scan rate of 0.01 V s^{-1} and within a potential range of 0.05 to -0.8 V *vs.* RHE.

2.4 Characterization

The surficial morphologies of the heat-treated metallic Ti and TiX (X: O_2, C, N) substrates were observed with scanning electron microscopy (SEM, XL30S FEG, PHILPS ELECTRON OPTICS B.V.) using a 5 kV accelerating voltage and 5 k resolution. Also, the crystal structures of each substrate sample were analyzed with X-ray diffraction (XRD, D/MAX-2500-PC, Rigaku). The synthesized Ru/TiC powder samples were analyzed by inductively coupled plasma mass spectrometry (ICP-MS, NexION 300s, Perkin Elmer) to be clarified about their mass fraction of Ru. Those mass fractions were used to prepare the catalyst solutions of the same amount of Ru. Oxidation states of Ru catalyst atom for 3 differently loaded Ru/TiC samples were analyzed with X-ray absorption near edge structure (XANES) using a synchrotron beam (Pohang Accelerator Laboratory (PAL), 8C Nano XAFS) to find out how oxidation state varies with the difference in the white line intensities.

3. Results and Discussion

3.1 Material characterizations for model catalyst

As substrates for TiC-supported Ru catalysts, we prepared Titanium compound (oxide, carbide, and nitride) pellets using a thermal decomposition method. Mechanically polished polycrystalline Ti pellets were annealed under the corresponding gaseous atmosphere. To confirm their phase and structure, we first conducted the XRD analysis of each annealed substrate pellet. Fig. 1 shows the XRD patterns of each substrate (metallic Ti, TiO_2, TiC, and TiN). As Ti-compound was partially grown in a preferred facet orientation during the annealing process, there was a slight difference in the relative intensity of JCPDS data and the measured XRD data. However, all high crystallinity Ti-compound substrates were successfully synthesized.

Meanwhile, unwanted titanium hydrides (TiH_2) may be formed during the TiC synthesis process with the gas decomposition method of CH_4 (Eq. 1 and 2) [31,32].

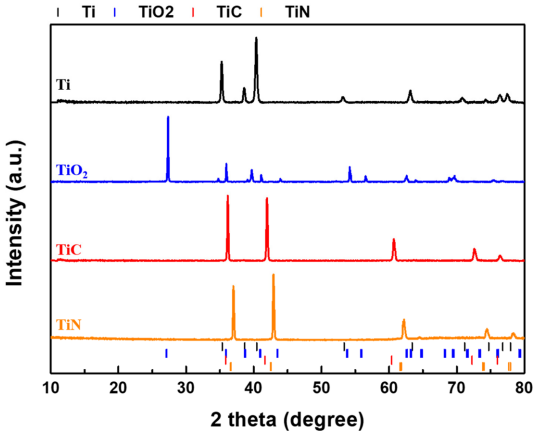

Fig. 1. XRD results of each Ti-compound substrate fabricated by thermal decomposition

$$CH_4 + Ti \rightarrow TiC + H_2 \quad (1)$$

$$Ti + H_2 \rightarrow TiH_2 \quad (2)$$

However, the XRD pattern of TiH_2 was not observed at the TiC XRD spectrum, confirming that TiH_2 impurity was removed by annealing after thermal decomposition. It is attributable that hydrides are easily decomposed under high vacuum and high-temperature conditions. The detailed peak positions of all XRD spectra and their relative intensities are summarized in Fig. S1 and Table S1.

To further investigate the surface structure of the substrate samples, we compared the SEM images of Ti, TiO_2, TiC, and TiN substrate. SEM images in Fig. 2 show that the polycrystalline Ti pellet has a mirror-like flat surface, while the other substrates have rough surfaces. As the rough surface of the Ti-compound substrate has a large electrochemical surface area, it can be advantageous in the perspective of electrochemical activity [33].

The CV test confirmed the enlarged electrochemical surface area of the Ti-compound substrate. Fig. S2 shows the CV profiles of each Ti-compound substrate in 1 M KOH. A pair of largely flat redox currents was observed for all CV curves, indicating that the double layer capacitance largely derives from the

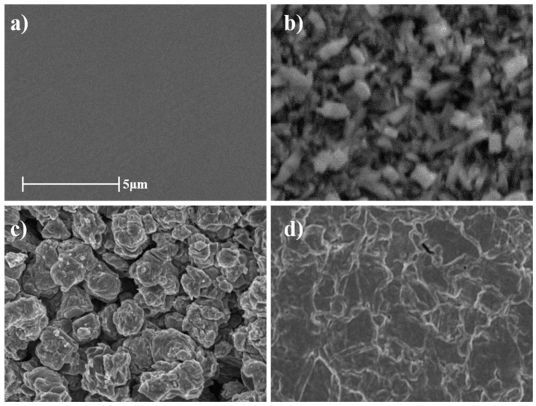

Fig. 2. SEM images of (a) metallic Ti, (b) TiO_2, (c) TiC, and (d) TiN

pseudocapacitance based on the reversible redox reaction of the electrode surface. The order of the CV integration area is as follows: TiC > TiN > TiO_2 > Ti. The CV integration area of TiC substrate was much larger than that of other substrates, especially tens of times larger than TiO_2. While the TiO_2 exhibited a highly rough surface similar to TiC, the electric resistivity of TiO_2 (10^{10}–10^{15} Ω m) is higher than that of TiC (0.003–0.008 Ω m) [34]. Taken all together, TiC is the most suitabl e Ti-compound substrate for electrocatalyst in which it has a large electrochemical surface area and high electrical conductivity.

3.2 HER performance test for model catalyst

Subsequently, we synthesized the Ti-compound supported Ru model catalyst using physical vapor deposition (Korea Vacuum Tech). An E-beam evaporation method was used for Ru deposition in which it has more precise controllability for nano units than other PVD types such as magnetron sputtering [35]. In this study, 1 nm of Ru was respectively deposited on Ti, TiO_2, TiN, TiC, and GC at a deposition rate of 0.01 nm s^{-1} for HER electrocatalyst. Polycrystalline Pt pellet (99.999%, diameter = 6.35 mm, Kurt J. Lesker Co. Ltd.) and Ru pellet (99.999%, diameter = 6.35 mm, Kurt J. Lesker Co. Ltd) were also prepared as a reference for comparison of HER activity.

The HER activity of the Ti-compound supported Ru model catalysts was measured in a KOH (1 M) alkaline electrolyte using a three-electrode electrochemical cell. LSV tests were carried out at a scan rate of 0.01 V s^{-1} and a potential range of 0.05 V to -0.8 V *vs.* RHE. As shown in Fig. 3a, the HER activity of Ru/TiX model catalysts was in the following order: Ru/TiO_2 < Ru/Ti < Ru/TiN < Ru/TiC, verifying the outstanding HER performance of Ru/TiC.

In particular, the HER overpotential of Ru/TiC at 10 mA cm^{-2} (55 mV) was lower than that of Ru on GC (171 mV, where GC is glassy carbon) and polycrystalline Ru (157 mV, see in Fig. S3), and a slightly higher than polycrystalline Pt (38 mV, see in Fig. S4). These results confirmed that the Ru/TiC catalysts developed here can be used as a substitute for Pt, especially when the cost difference between Ru (Ru = \$17 g^{-1}, Mar 2022) and Pt (Ru = \$34 g^{-1}, Mar 2022) is considered. The current densities of each catalyst at a potential of -0.1 V *vs.* RHE for HER activity comparison were summarized in Fig. 3b.

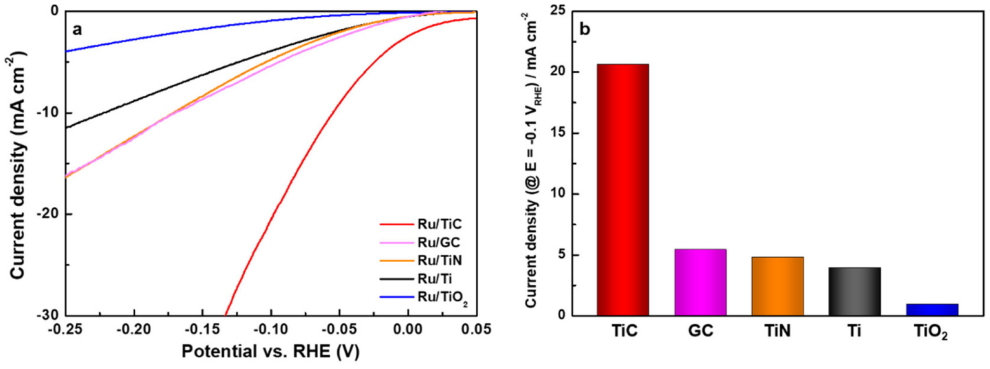

Fig. 3. (a) LSV plots and (b) corresponding current density graph (at -0.1 V *vs.* RHE) of alkaline HER tests for model catalyst Ru/Ti(X) (X = O_2, C, N) samples. Electrochemical tests were conducted in KOH (1 M) electrolyte (pH = 14) with Hg/HgO and a graphite rod as reference and counter electrodes, respectively

3.3 Material characterization for powder catalyst

The remarkable HER performance of the Ru/TiC catalyst in alkaline media can be affected by two effects: (1) the effect of large surface area for TiC substrate, (2) the effect of a metal-support interaction between Ru metal catalyst and TiC support. Furthermore, these effects are not mutually exclusive are addressed simultaneously. As demonstrated in sections 3.1 and 3.2, the high roughness of TiC substrate increases the available reaction sites, which improves the electrochemical performance. However, it is unclear whether the improved HER performance of the Ru/TiC is caused by the metal-support interactions between Ru metal catalyst and TiC support. To clearly observe in view of metal-support interaction, we finally synthesized a powder-based catalyst that minimizes the difference in electrochemical surface area.

The powder-based Ru/TiC catalysts were synthesized through simple powder sputtering onto a TiC nanopowder with particle size ranging within 200 nm. The weight percent of Ru to the total catalyst was determined by the sputtering time, and the Ru content in each powder-sputtered Ru/TiC sample was calculated by ICP-MS. Table 1 was summarized the ICP-MS results of each Ru-deposited powder sample. Based on the measured Ru content in each sample, the deposition rate of Ru showed a linear trend with the increase in the deposition time.

To further investigate the influence of the TiC support on the Ru oxidation states, we additionally performed the X-ray adsorption spectroscopy analysis with a synchrotron beam (Pohang Accelerator Laboratory (PAL), 8C Nano XAFS). As the characterization of Ru oxidation states is important to understand water splitting catalysis [23], we focused on analyzing the oxidation state of the powder-based Ru/TiC catalysts based on the previously reported Ru-K edge reference data as well as that of our metallic Ru data [36,37].

Fig. 4 shows the normalized Ru K-edge XANES spectra of each sample, including the bare Ru foil used as a reference. To give a direct comparison of the oxidation state of Ru in the Ru/TiC samples, we acquired the Ru oxidation state as a function of Ru K-edge energy shift (the edge position defined as the energy at which absorption = 0.5) with the previously reported Ru-K edge reference data and our metallic Ru data [36,37](Fig. S5). The oxidation state of Ruthenium in the Ru/TiC samples is found to vary from 2.4 (Ru/TiC_3.92%) to 3.8 (Ru/TiC_0.56%), which is attributable to metal-support interaction. As the Ru loading of Ru/TiC powder catalyst was increased, the edge position and the white-line peak position were red-shifted, indicating that the oxidation state of Ru on the TiC substrate was gradually decreased with the increment of the Ru loading. Assuming that the Ru deposition time is more than 12 minutes, the XANES spectrum for Ru/TiC would finally be converged to that of a bulk-like nanoparticle structure, like metallic Ru. All Ru-K edge XANES results were summarized in Table S2.

3.4 HER performance test for powder catalyst

To investigate the effects of the interaction between the catalyst and the support, the investigation of electrocatalytic hydrogen evolution reaction activities of Ru/TiC powder catalysts under alkaline media was

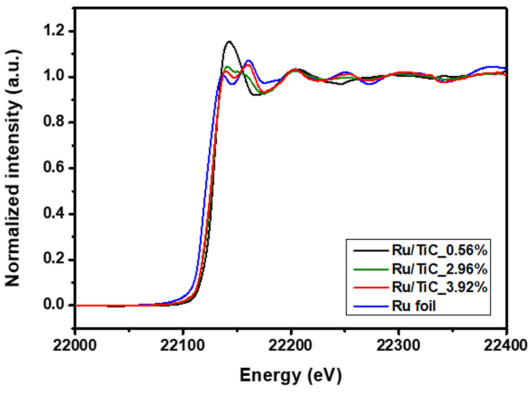

Fig. 4. XANES results of Ru/TiC powder samples using Ru foil as a reference

Table 1. ICP-MS results of the powder-sputtered Ru/TiC samples

Sample	Ti (ppb)	Ru (ppb)	Ti:Ru	wt%
Ru 3 min on TiC	214.4984	0.7163	302:1	0.56
Ru 9 min on TiC	136.6756	2.3941	57:1	2.96
Ru 12 min on TiC	190.0494	4.4052	43:1	3.92

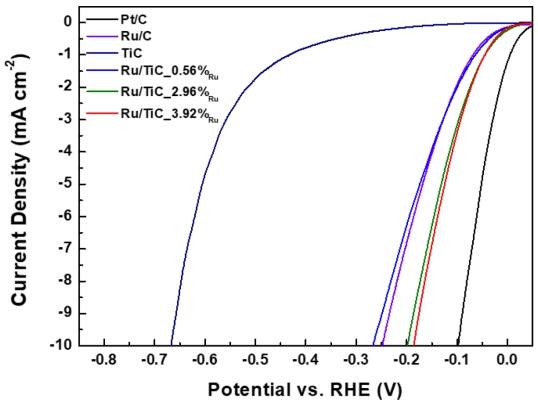

Fig. 5. LSV plots of alkaline HER tests for powder catalyst samples prepared by powder sputtering. Electrochemical tests were conducted in KOH (1 M) electrolyte (pH = 14) with Hg/HgO and a graphite rod as reference and counter electrodes, respectively

finally conducted in the same three-electrode system in 1 M KOH. For comparison, Pt/C (20 wt%) and Ru/C (5 wt%) were also prepared as a reference for the electrochemical tests. Fig. 5 shows the results of the electrochemical tests of the powder samples. The HER overpotential of powder catalysts at 10 mA cm^{-2} was in the following order: Pt/C (100 mV) < Ru/TiC_3.92%$_{Ru}$ (12 min, 184 mV) < Ru/TiC_2.96%$_{Ru}$ (9 min, 198 mV) < Ru/C (250 mV) < Ru/TiC_0.56%$_{Ru}$ (3 min, 266 mV) < TiC (665 mV). While the sample prepared over a 3-min Ru deposition time (0.56 wt%) exhibited a slightly lower activity than Ru/C, those prepared over deposition times of 9 min (2.96 wt%) and 12 min (3.92 wt%) exhibited better activities. It suggests that using a Ru/TiC catalyst with the Ru loading approximately from 3 to 4 wt% generates the enhanced HER activity due to the appropriate metal-support interaction.

4. Conclusions

In summary, the Ru/TiC catalyst proposed here exhibited much better performance than metallic Ru for HERs in alkaline media, even at significantly small Ru loadings. The electrochemical tests on the model catalysts indicated that Ru/TiC has a low HER overpotential (55 mV) at 10 mA cm^{-2}, which is comparable to that of metallic Pt and much better than that of metallic Ru. The characterization and HER tests conducted on Ru/TiC powder catalysts confirmed that its high catalytic performance could be attributed to the high surface area of the TiC substrate and the metal–support interaction between Ru and TiC. Additionally, Ru is more cost-effective than Pt, especially as the Ru content used in the catalyst is extremely small. Thus, using the Ru/TiC catalyst can significantly reduce the overall cost of the alkaline water-electrolysis cells. Taken all together, this TiC-supported Ru catalyst with a metal-support interaction can be a possible alternative to Pt catalysts to reduce the total cost of the system of water electrolyzer considerably.

Acknowledgements

This work was supported by the grants from National Research Foundation of Korea (2019M3D1A1079306) and Korea Electric Power Corporation (R20XO02-31).

Supporting Information

Supporting Information is available at https://doi.org/10.33961/jecst.2022.00178

References

[1] S.-M. Jung, S.-W. Yun, J.-H. Kim, S.-H. You, J. Park, S. Lee, S. H. Chang, S. C. Chae, S. H. Joo, Y. Jung, J. Lee, J. Son, J. Snyder, V. Stamenkovic, N. M. Markovic, and Y.-T. Kim, *Nat. Catal.*, **2020**, *3(8)*, 639-648.
[2] S.-M. Jung, J. Kwon, J. Lee, K. Shim, D. Park, T. Kim, Y. H. Kim, S. J. Hwang, Y.-T. Kim, and Y.-T. Kim, *ACS Appl. Energy Mater.*, **2020**, *3(7)*, 6383-6390.
[3] W. Kuckshinrichs, T. Ketelaer, and J. C. Koj, *Front. Energy Res.*, **2017**, *5*, 1.
[4] N. Cheng, S. Stambula, D. Wang, M. N. Banis, J. Liu, A. Riese, B. Xiao, R. Li, T. K. Sham, L. M. Liu, G. A. Botton, and X. Sun, *Nat. Commun.*, **2016**, *7*, 13638.
[5] J. Zhang, Y. Zhao, X. Guo, C. Chen, C.-L. Dong, R.-S. Liu, C.-P. Han, Y. Li, Y. Gogotsi, and G. Wang, *Nat. Catal.*, **2018**, *1(12)*, 985-992.
[6] D. V. Esposito, S. T. Hunt, A. L. Stottlemyer, K. D. Dobson, B. E. McCandless, R. W. Birkmire, and J. G. Chen, *Angew. Chem. Int. Ed.*, **2010**, *49(51)*, 9859-9862.
[7] M. Tavakkoli, N. Holmberg, R. Kronberg, H. Jiang, J. Sainio, E. I. Kauppinen, T. Kallio, and K. Laasonen, *ACS Catal.*, **2017**, *7(5)*, 3121-3130.
[8] D. Voiry, H. Yamaguchi, J. Li, R. Silva, D. C. Alves, T. Fujita, M. Chen, T. Asefa, V. B. Shenoy, G. Eda, and M. Chhowalla, *Nat. Mater.*, **2013**, *12(9)*, 850-855.
[9] M. Gong, W. Zhou, M. C. Tsai, J. Zhou, M. Guan, M. C. Lin, B. Zhang, Y. Hu, D. Y. Wang, J. Yang, S. J.

Pennycook, B. J. Hwang, and H. Dai, *Nat. Commun.*, **2014**, *5*, 4695.
[10] J. Kibsgaard and T. F. Jaramillo, *Angew. Chem. Int. Ed.*, **2014**, *53(52)*, 14433-14437.
[11] C. Wan, Y. N. Regmi, and B. M. Leonard, *Angew. Chem. Int. Ed.*, **2014**, *53(25)*, 6407-6410.
[12] J. Kim, H. Jung, S.-M. Jung, J. Hwang, D. Y. Kim, N. Lee, K.-S. Kim, H. Kwon, Y.-T. Kim, J. W. Han, and J. K. Kim, *J. Am. Chem. Soc.*, **2020**, *143(3)*, 1399-1408.
[13] P. Quaino, F. Juarez, E. Santos, and W. Schmickler, *Beilstein J. Nanotechnol.*, **2014**, *5(1)*, 846-854.
[14] S. Trasatti, *J. Electroanal. Chem. Interf. Electrochem.*, **1972**, *39(1)*, 163-184.
[15] Y. Lee, J. Suntivich, K. J. May, E. E. Perry, and Y. Shao-Horn, *J. Phys. Chem. Lett.*, **2012**, *3(3)*, 399-404.
[16] Z. Pu, I. S. Amiinu, Z. Kou, W. Li, and S. Mu, *Angew. Chem. Int. Ed.*, **2017**, *56(38)*, 11559-11564.
[17] J. Wang, Z. Wei, S. Mao, H. Li, and Y. Wang, *Energy Environ. Sci.*, **2018**, *11(4)*, 800-806.
[18] J. Feng, F. Lv, W. Zhang, P. Li, K. Wang, C. Yang, B. Wang, Y. Yang, J. Zhou, and F. Lin, *Adv. Mater.*, **2017**, *29(47)*, 1703798.
[19] P. Quaino, E. Santos, H. Wolfschmidt, M. Montero, and U. Stimming, *Catalysis today*, **2011**, *177(1)*, 55-63.
[20] M. E. Björketun, G. S. Karlberg, J. Rossmeisl, I. Chorkendorff, H. Wolfschmidt, U. Stimming, and J. K. Nørskov, *Phys. Rev. B*, **2011**, *84(4)*, 045407.
[21] P. J. Schäfer and L. A. Kibler, *Phys. Chem. Chem. Phys.*, **2010**, *12(46)*, 15225-15230.
[22] S.-Y. Bae, J. Mahmood, I.-Y. Jeon, and J.-B. Baek, *Nanoscale Horiz.*, **2020**, *5(1)*, 43-56.
[23] Y. Zheng, Y. Jiao, Y. Zhu, L. H. Li, Y. Han, Y. Chen, M. Jaroniec, and S.-Z. Qiao, *J. Am. Chem. Soc.*, **2016**, *138(49)*, 16174-16181.
[24] Shanghai Metals Market. https://price.metal.com/Other-Precious-Metals (accessed 26 November 2021).
[25] Z.-F. Huang, J. Song, K. Li, M. Tahir, Y.-T. Wang, L. Pan, L. Wang, X. Zhang, and J.-J. Zou, *J. Am. Chem. Soc.*, **2016**, *138(4)*, 1359-1365.
[26] D. Strmcnik, P. P. Lopes, B. Genorio, V. R. Stamenkovic, and N. M. Markovic, *Nano Energy*, **2016**, *29*, 29-36.
[27] X. Wang, R. Kumar, and D. J. Myers, *Electrochem. Solid-State Lett.*, **2006**, *9(5)*, A225.
[28] F. Kodera, Y. Kuwahara, A. Nakazawa, and M. Umeda, *J. Power Sources*, **2007**, *172(2)*, 698-703.
[29] W. Sheng, H. A. Shao-Horn, and S.-H. Yang, *J. Electrochem. Soc.*, **2010**, *157(11)*, B1529.
[30] J. Mahmood, F. Li, S.-M. Jung, M. S. Okyay, I. Ahmad, S.-J. Kim, N. Park, H. Y. Jeong, and J.-B. Baek, *Nat. nanotechnol.*, **2017,** *12(5)*, 441-446.
[31] B.-J. Lee, S.-M. Jung, J. Kwon, J. Lee, K.-S. Kim, and Y.-T. Kim, *ACS Appl. Energy Mater.*, **2022**, *5(2)*, 2130-2137.
[32] Y.-J. Kim, H. Chung, and S.-J. Kang, *Compos. Part A: Appl. Sci. Manuf.*, **2001**, *32(5)*, 731-738.
[33] C. C. McCrory, S. Jung, J. C. Peters, and T. F. Jaramillo, *J. Am. Chem. Soc.*, **2013,** *135(45)*, 16977-16987.
[34] J. F. Shackelford, Y.-H. Han, S. Kim, and S.-H. Kwon, *CRC materials science and engineering handbook, 4th Ed.*, CRC press, **2016**.
[35] N. Selvakumar and H. C. Barshilia, *Sol. Energy Mater. Sol. Cells*, **2012**, *98*, 1-23.
[36] C. I. Hiley, M. R. Lees, J. M. Fisher, D. Thompsett, S. Agrestini, R. I. Smith, and R. I. Walton, *Angew. Chem. Int. Ed.*, **2014**, *53(17)*, 4423-4427.
[37] K. Sardar, E. Petrucco, C. I. Hiley, J. D. Sharman, P. P. Wells, A. E. Russell, R. J. Kashtiban, J. Sloan, and R. I. Walton, *Angew. Chem. Int. Ed.*, **2014**, *53(41)*, 10960-10964.